energies

MDPI

Article

Study on Winding Inductances in Stator Surface-Mounted Permanent Magnet Machines

Xiaofeng Zhu * and Yan Yue

School of Electrical and Automation Engineering, Nanjing Normal University, Nanjing 210023, China; yueyan9908@163.com
* Correspondence: zhuxf@njnu.edu.cn

Abstract: Winding inductance always plays a key role in the electromagnetic performances of stator surface-mounted permanent magnet (SSPM) machines, including their flux-weakening capability, prospective fault current, power factor, current ripple, etc. Generally speaking, winding inductance mainly comprises three components: an air-gap component, a slot-leakage component, and an end-leakage component. In this paper, firstly, the winding pole pairs of SSPM machines are investigated based on the magneto-motive force-permeance model, through which the winding configurations can also be determined. Then, according to the winding configurations, three analytical expressions for each inductance component are derived to evaluate the winding inductance per phase. In addition, finite element analysis (FEA) is employed to verify the effectiveness of the derived analytical expressions. Meanwhile, three prototyped SSPM machines are manufactured, and their winding inductances are measured to further verify the analytical expressions. The measured results agree with both the analytical and FEA results very well.

Keywords: stator surface-mounted permanent magnet machine; inductance; analytical; finite element analysis

check for updates

Citation: Zhu, X.; Yue, Y. Study on Winding Inductances in Stator Surface-Mounted Permanent Magnet Machines. *Energies* **2024**, *17*, 5359. https://doi.org/10.3390/en17215359

Academic Editor: Adolfo Dannier

Received: 1 October 2024
Revised: 15 October 2024
Accepted: 22 October 2024
Published: 28 October 2024

Copyright: © 2024 by the authors. Licensee MDPI, Basel, Switzerland. This article is an open access article distributed under the terms and conditions of the Creative Commons Attribution (CC BY) license (https://creativecommons.org/licenses/by/4.0/).

1. Introduction

The conventional permanent magnet (PM) brushless machine is widely utilized for industrial applications, including wind power generators, servo systems, in-wheel motors, compressors, etc. [1–7], where the PMs are always housed in the rotor side (Figure 1a) and named as rotor-PM machines. However, in rotor-PM machines, the retaining sleeve is usually necessary to protect the PMs from the centrifugal force, which correspondingly results in a more complicated manufacture. In addition, a rising rotor temperature due to poor thermal dissipation is another challenge since it may cause the undesired irreversible demagnetization of PMs, degrading machine performance. Hence, in order to avoid these problems, more and more scholars have begun to pay attention to a new type of PM machine that moves the PMs from rotor to stator, namely a stator surface-mounted (SS) PM machine [4,8–11].

Generally speaking, the SSPM machine can be classified into three major categories according to the number and magnetization method of PMs belonging to the same stator tooth, as shown in Figure 1b–d. It is easy to find from Figure 1b that there is only a single PM located in each stator tooth, named SSPM machine 1. Thus, the PM flux linked in each coil is unipolar [10,11]. However, in Figure 1c,d, a pair of PMs with reversal polarities are mounted on the surface of each stator tooth. Hence, they are also called flux-reversal (FR) PM machines. The only difference between the two machines in Figure 1c,d is the magnetization mode. As can be seen, the adjacent PMs belonging to the neighbor stator tooth have the same polarity (SSPM machine 2, mode 1) in Figure 1c, while reversal polarity (SSPM machine 3, mode 2) can be seen in Figure 1d. Clearly, the PM flux linkage of each coil in the two FRPM machines is bipolar.

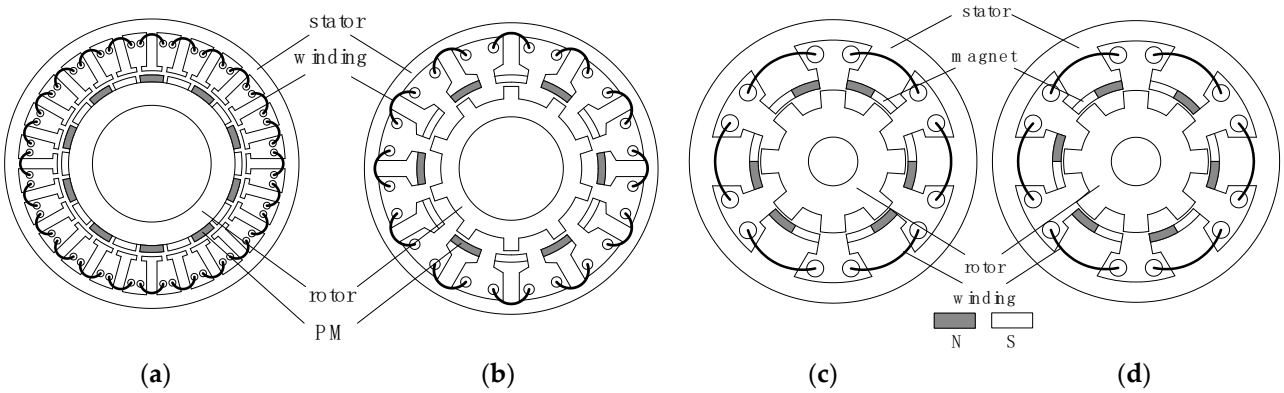


Figure 1. SSPM and RSPM machines. (**a**) RSPM machine. (**b**) SSPM machine 1. (**c**) SSPM machine 2. (**d**) SSPM machine 3.

From previous studies, it is easy to find that most scholars pay attention to such aspects, including machine optimization [12–20], especially on cogging torque reduction [15–20], while others try to propose some general procedures that should be considered during the machine design stage [21,22]. However, few researchers devote themselves to studying winding inductance, which always plays a key role in the electromagnetic performance of SSPM machines, including flux-weakening capability, prospective fault current, power factor, current ripple [23,24], etc.

In general, the winding inductance of one phase, namely phase inductance, can be classified into two categories: phase self-inductance and phase mutual inductance. Meanwhile, both categories can be further considered to have three components: the air-gap component, the slot-leakage component, and the end-leakage component. There are quite a large number of studies that focus on the inductance of conventional electrical machines [25–28], such as interior PM machines, rotor-SPM machines, induction machines, etc. However, the inductive characteristic of SSPM machines is different due to their special magnetic circuit.

Hence, the purpose of this paper is to create a better understanding of winding inductances in such SSPM machines. Then, a possible control strategy can be used. In Section 2, winding configurations and winding pole pairs are investigated based on the magnetomotive force (MMF)-permeance model. Then, according to the winding configurations, three analytical expressions for each inductance component are derived to evaluate the phase inductance in Section 3. In addition, finite element analysis (FEA) is employed to verify the effectiveness of the derived analytical expressions. Meanwhile, three prototyped machines are manufactured, and their phase inductances are measured to further verify the analytical expressions in Section 4. Finally, some conclusions are drawn in Section 5.

2. Winding Pole Pairs and Winding Configurations

Winding pole pairs have a great effect on winding configurations and, hence, inductance. That is to say, winding pole pairs should be determined before the analysis of inductance. For the interest of simplicity, three assumptions are made before the following derivations: (1) the permeability of the iron core is supposed to be infinite, (2) flux leakage is negligible, and (3) the variation in the magnetic field is in the radial direction only.

2.1. Winding Pole Pairs

Thus, based on the assumption mentioned above, the MMF due to PMs only and magnetic permeance for each machine can be expressed, as shown in Figure 2. Clearly, though they have different PM-MMF models, the permeance model is the same.

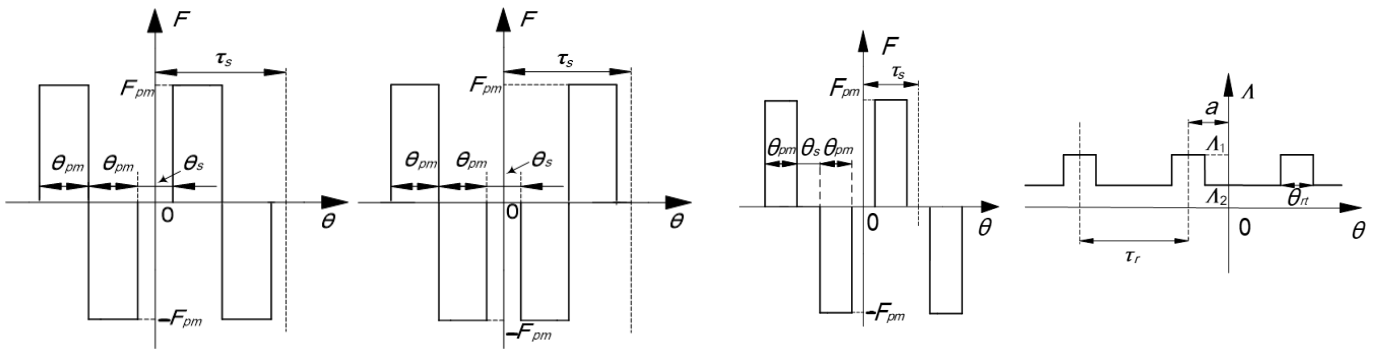


Figure 2. MMF and permeance. (**a**) MMF (SSPM machine 1). (**b**) MMF (SSPM machine 2). (**c**) MMF (SSPM machine 3). (**d**) Permeance.

According to Figure 2a, the PM-MMF distribution of SSPM machine 1 can be written as follows:

$$F_1 = \begin{cases} 0, & 0 < \theta \le \frac{\theta_s}{2} \\ F_{pm}, & \frac{\theta_s}{2} < \theta \le \frac{\theta_s}{2} + \theta_{pm} \\ 0, & \frac{\theta_s}{2} + \theta_{pm} < \theta \le \tau_s + \frac{\theta_s}{2} \\ -F_{pm}, & \tau_s + \frac{\theta_s}{2} < \theta \le 2\tau_s - \frac{\theta_s}{2} \\ 0, & 2\tau_s - \frac{\theta_s}{2} < \theta \le 2\tau_s \end{cases} \quad (1)$$

where θ, θ_s, and θ_{pm} are the widths of the stator location, stator slot, and PMs in the circumferential direction, respectively; F_{pm} is magnet MMF, τ_s is the stator pole-pitch, $\tau_s = \frac{2\pi}{N_s}$, and N_s is the stator pole number.

By using Fourier analysis, Equation (1) becomes

$$F_1 = \sum_{n_1=1}^{\infty} F_{n_1} \sin \frac{n_1 N_s \theta}{2},\ n_1 = 1,\ 3,\ 5 \ldots \quad (2)$$

where $F_{n_1} = \frac{4F_{pm}}{n_1 \pi} \cos(\frac{n_1 N_s \theta_s}{4})$, n_1 is the harmonic order of MMF.

Similarly, the PM-MMF of SSPM machine 2 yields the following:

$$F_2 = \begin{cases} 0, & 0 < \theta \le \frac{\theta_s}{2} \\ -F_{pm}, & \frac{\theta_s}{2} < \theta \le \frac{\theta_s}{2} + \theta_{pm} \\ F_{pm}, & \frac{\theta_s}{2} + \theta_{pm} < \theta \le \tau_s - \frac{\theta_s}{2} \\ 0, & \tau_s - \frac{\theta_s}{2} < \theta \le \tau_s + \frac{\theta_s}{2} \\ F_{pm}, & \tau_s + \frac{\theta_s}{2} < \theta \le \tau_s + \frac{\theta_s}{2} + \theta_{pm} \\ -F_{pm}, & \tau_s + \frac{\theta_s}{2} + \theta_{pm} < \theta \le 2\tau_s - \frac{\theta_s}{2} \\ 0, & 2\tau_s - \frac{\theta_s}{2} < \theta \le 2\tau_s \end{cases} \quad (3)$$

Equation (2) also can be written as a Fourier series:

$$F_2 = \sum_{n_2=1}^{\infty} F_{n_2} \cos \frac{n_2 N_s \theta}{2},\ n_2 = 1,\ 3,\ 5 \ldots \quad (4)$$

where $F_{n_2} = \frac{4F_{pm}}{n_2 \pi} [(-1)^{\frac{n_2+1}{2}} + \sin(\frac{n_2 N_s \theta_s}{4})]$, n_2 is the harmonic order of MMF.

Finally, the PM-MMF of SSPM machine 3 satisfies the following:

$$F_3 = \begin{cases} 0, & 0 < \theta \le \frac{\theta_s}{2} \\ F_{pm}, & \frac{\theta_s}{2} < \theta \le \frac{\theta_s}{2} + \theta_{pm} \\ -F_{pm}, & \frac{\theta_s}{2} + \theta_{pm} < \theta \le \tau_s - \frac{\theta_s}{2} \\ 0, & \tau_s - \frac{\theta_s}{2} < \theta \le \tau_s \end{cases} \quad (5)$$

It also can be written as a Fourier series:

$$F_3 = \sum_{n_3=1}^{\infty} F_{n_3} \sin n_3 N_s \theta,\ n_3 = 1,\ 2,\ 3 \ldots \tag{6}$$

where $F_{n_3} = \frac{2F_{pm}}{n_3 \pi}[1 - \cos(n_3 N_s \theta_{pm})]$ and n_3 is the harmonic order of MMF.

The magnetic permeance model of these three SSPM machines has the same formula, and it can be expressed as follows:

$$\Lambda(\theta, \alpha) \approx \Lambda_0 + \Lambda_r \cos N_r(\theta + \alpha) \tag{7}$$

where N_r is the rotor pole number and α is the angle of the rotor position relative to θ. Λ_0 and Λ_m are Fourier coefficients and $\Lambda_0 = \frac{N_r}{2\pi}[(\tau_r - \theta_{rt})\Lambda_2 + \theta_{rt}\Lambda_1]$, $\Lambda_r = \frac{2(\Lambda_1 - \Lambda_2)}{\pi} \sin(\frac{N_r \theta_{rt}}{2})$, and θ_{rt} is rotor tooth width, τ_r is the rotor pole-pitch, and $\tau_r = \frac{2\pi}{N_r}$, N_r is the rotor pole number.

Therefore, the air-gap flux density due to PMs only can be obtained by employing Equation (8):

$$B(\theta, \alpha) = F \cdot \Lambda(\theta, \alpha) \tag{8}$$

Thus, the PM air-gap flux density of SSPM machine 1 is as follows:

$$B_1 = \sum_{n_1=1}^{\infty} \Lambda_0 F_{n_1} \sin \frac{n_1 N_s \theta}{2} + \sum_{n_1=1}^{\infty} \Lambda_r F_{n_1} \sin \frac{n_1 N_s \theta}{2} \cos N_r(\theta + \alpha) \tag{9}$$

Clearly, the first term of Equation (9) is static, and it has no effect on electromechanical energy conversion. Hence, this term can be omitted, and Equation (9) can be rewritten as follows:

$$B_1 = \sum_{n_1=1}^{\infty} \Lambda_r F_{n_1} \sin \frac{n_1 N_s \theta}{2} \cos N_r(\theta + \alpha) = \sum_{n_1=1}^{\infty} \frac{\Lambda_r F_{n_1}}{2} \sin[\frac{(n_1 N_s \pm 2N_r)\theta}{2} \pm N_r \alpha] \tag{10}$$

Similarly, the PM air-gap flux density of SSPM machines 2 and 3 is

$$B_2 = \sum_{n_2=1}^{\infty} \Lambda_r F_{n_2} \cos \frac{n_2 N_s \theta}{2} \cos N_r(\theta + \alpha) = \sum_{n_2=1}^{\infty} \frac{\Lambda_r F_{n_2}}{2} \cos[\frac{(n_2 N_s \pm 2N_r)\theta}{2} \pm N_r \alpha] \tag{11}$$

$$B_3 = \sum_{n_3=1}^{\infty} \Lambda_r F_{n_3} \sin n_3 N_s \theta \cdot \cos N_r(\theta + \alpha) = \sum_{n_3=1}^{\infty} \frac{\Lambda_r F_{n_3}}{2} \cos[(n_3 N_s \pm N_r)\theta \pm N_r \alpha] \tag{12}$$

Thus, the corresponding PM flux linkage per phase can be expressed as follows [21,22]:

$$\psi = r_g L_a \int_0^{2\pi} B(\theta, \alpha) N(\theta) d\theta \tag{13}$$

where r_g is the mean air-gap radius, L_a is the effective length, and $N(\theta)$ is the winding function of a single phase, which can be written as follows:

$$N(\theta) = \sum_{m=1}^{\infty} N_m \cos mP\theta,\ m = 1,\ 3,\ 5 \ldots \tag{14}$$

where P stands for winding pole pairs.

Substituting Equations (10) and (14) into Equation (13), the corresponding phase PM flux linkage of SSPM machine 1 is the following:

$$\psi_1 = r_g L_a \sum_{n_1=1}^{\infty} \sum_{m_1=1}^{\infty} \int_0^{2\pi} \frac{\Lambda_r F_{n_1}}{2} \sin[\frac{(n_1 N_s \pm 2N_r)\theta}{2} \pm N_r \alpha] N_{m_1} \cos m_1 P_1 \theta \tag{15}$$

It is clear that the following equation should be met, or Equation (15) would always be 0:

$$\frac{n_1 N_s \pm 2N_r}{2} = m_1 P_1 \text{ or } P_1 = \frac{n_1 N_s \pm 2N_r}{2m_1} \tag{16}$$

Similarly, the winding pole pairs of SSPM machines 2 and machine 3 are the following:

$$P_2 = \frac{n_2 N_s \pm 2N_r}{2m_2} \tag{17}$$

$$P_3 = \frac{n_3 N_s \pm N_r}{m_3} \tag{18}$$

2.2. Winding Configurations

According to Equations (16)–(18), the winding pole pairs and winding configuration for each machine are obtained. For example, P_1 is calculated to be four for SSPM machine 1 with 12 stator slots and 10 rotor poles (12/10) based on equation (16). Thus, the coils belonging to phase A have the same polarity, as do phases B and C, as shown in Figure 3a. In using this winding configuration, the FEA-predicted flux distribution induced by phase A is shown in Figure 3b, where four pole pairs exist, consistent with the above analysis. Similarly, the winding configurations of machines 2 (6/8) and 3 (6/8), as well as their flux distributions, are obtained, as shown in Figure 3c–f.

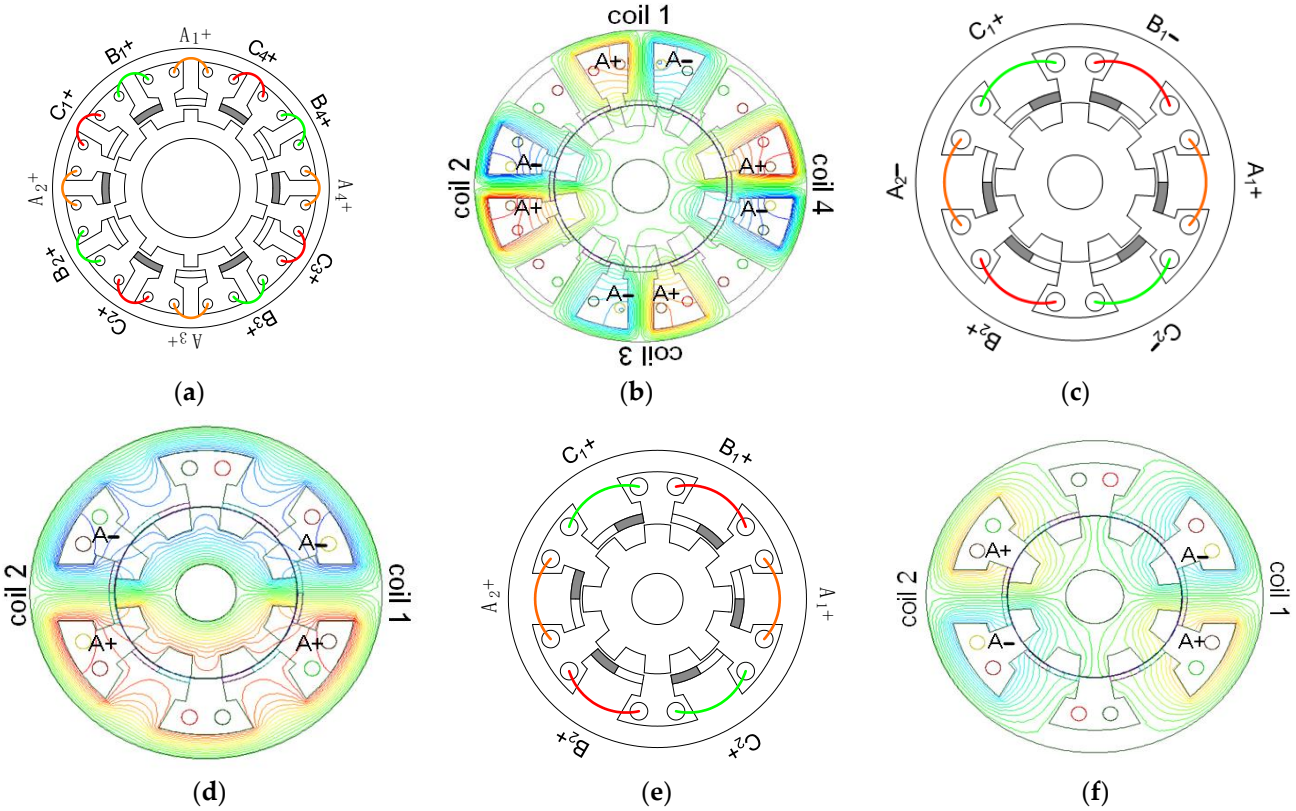


Figure 3. Winding configurations and flux distributions. (**a**) Winding configuration (machine 1). (**b**) Flux distribution (machine 1). (**c**) Winding configuration (machine 2). (**d**) Flux distribution (machine 2). (**e**) Winding configuration (machine 3). (**f**) Flux distribution (machine 3).

3. Winding Induction Calculation

As mentioned in Section 1, the main components of phase inductance include the air-gap component, the slot-leakage component, and the end-leakage component, which are calculated in this section. Though the winding configuration of each SSPM machine is different, the phase inductance calculation is nearly the same.

3.1. Air-Gap Component

(1) Self-inductance

In general, the SSPM machine can be considered a non-salient pole PM machine [9–11], i.e., the winding inductance is independent of the rotor position. Hence, the position where the rotor tooth aligns with the stator tooth is chosen to analyze the air-gap component (Figure 4). If the coil conductors per slot that belong to one phase are N_c, the total MMF due to armature currents around a complete flux path is equal to $qN_c i$, where q is the coil

number embraced by the flux path and i is the input current. As seen from Figure 4, q is equal to one for machines 1 and 3, while q is two for machine 2. Then, supposing that the permeability of silicon steel in both the stator and rotor is infinite, the MMF is concentrated across two effective air gaps, and hence, the MMF drop across each air gap is $F_g = qN_c i/2$. If the flux is assumed to radially cross the air gap, the magnetic field strength H in each air gap is

$$H = \frac{qN_c i}{2g'} \tag{19}$$

where g' is the effective air-gap length, and this is given by

$$g' = g + \frac{h_m}{\mu_r} \tag{20}$$

where h_m is magnet thickness and μ_r is relative permeability.

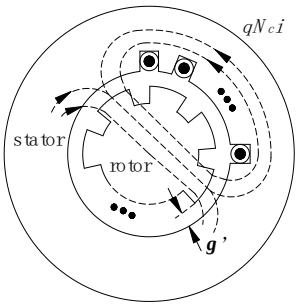


Figure 4. Air-gap component calculation.

Thus, the flux linked by one phase is as follows:

$$\psi_{ph} = \frac{\mu_0 q N_c i}{2g'} \cdot \theta_{st} r_{st} L_a \tag{21}$$

where μ_0 is the permeability of the vacuum, L_a is the lamination length, r_{st} is the stator inner radius, and θ_{st} is the stator tooth width.

Therefore, the air-gap component of self-inductance is as follows:

$$L_g = \frac{N_s}{3} \frac{\mu_0 q {N_c}^2}{2g'} \cdot \theta_{st} r_{st} L_a = \frac{\mu_0 q N_c N}{2g'} \cdot \theta_{st} r_{st} L_a \tag{22}$$

where N denotes the series of turns per phase.

(2) Mutual inductance

Mutual inductance in SSPM machines is different due to various winding configurations. As can be inferred from Figure 3c,d, the flux induced by phase A in machine 2 only links itself without linking any other phases, neither phase B nor phase C. Thus, the mutual inductance (air-gap component) between phases for machine 2 can be neglected.

However, strong coupling between phases exists in both machines 1 and 3. It is true that only one coil side produces the flux that will link the other phases. For example, the flux due to coil side A+ (coil 1) only links phase B, while flux due to the other coil side A− only links phase C. Therefore, the flux linkage of phase B (or phase C) induced by phase A is as follows:

$$\psi_{phmutual} = \frac{\mu_0 q N_c i}{4g'} \cdot \theta_{rt} r_{rt} L_a \tag{23}$$

Then, the air-gap component of mutual inductance either for machine 1 or 3 is the following:

$$M_g = \frac{N_s}{3} \frac{\mu_0 q {N_c}^2}{4g'} \cdot \theta_{rt} r_{rt} L_a = \frac{\mu_0 q N_c N}{4g'} \cdot \theta_{rt} r_{rt} L_a = \frac{L_g}{2} \tag{24}$$

Clearly, the self-inductance of the air-gap component for three SSPM machines can be calculated from Equation (22). However, the mutual inductance is different. For machine 2, the mutual component is nearly zero, while for both machines 1 and 3, the mutual inductance is half of the self-inductance.

The validation of the above conclusion can be given by 2D-FEA, as shown in Figure 5. It should be noted that only phase A is excited by a DC current of 5A. Thus, the flux linkages induced in all phases are caused by phase A only, i.e., self-flux linkage for phase A and mutual-flux linkage for both phases B and C. It is easy to find from either Figure 5a or c that the mutual flux linkages induced in phase B and phase C are completely the same, and they are half the self-flux linkage in phase A. As for machine 2, namely Figure 5b, the mutual flux linkage is nearly zero, which supports the aforementioned analysis.

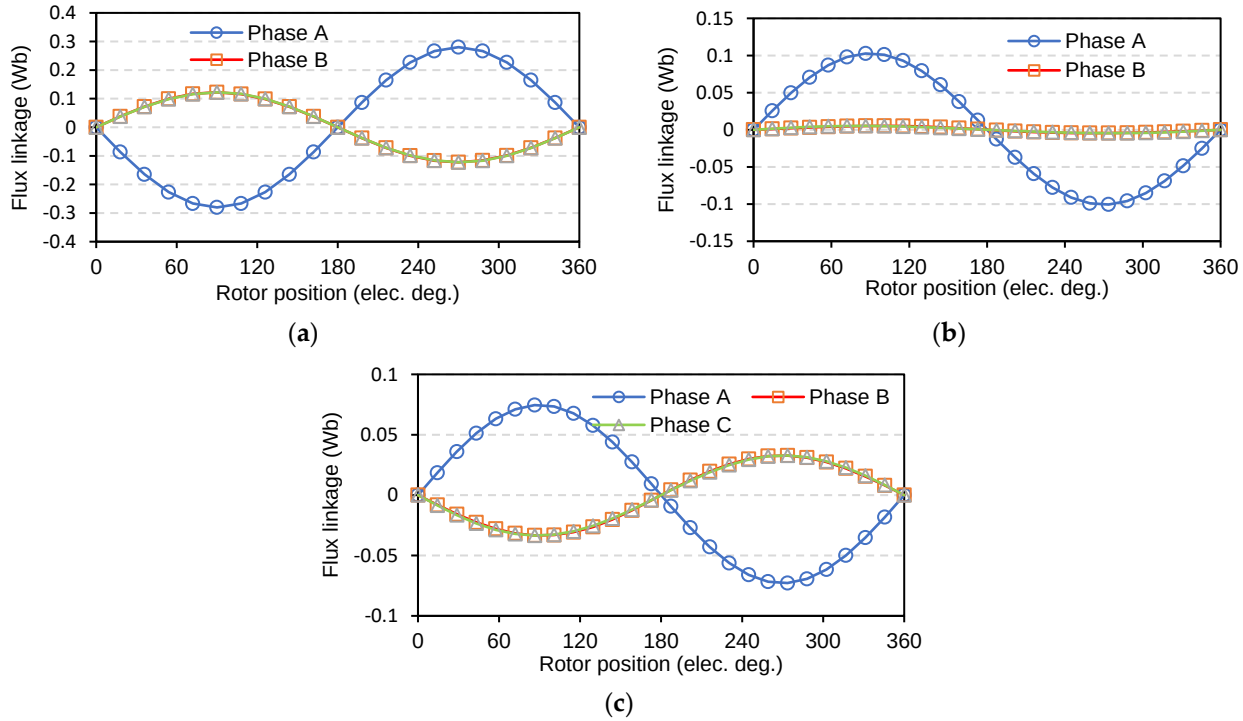


Figure 5. Three-phase flux linkages due to the current of phase A only. (**a**) Machine 1. (**b**) Machine 2. (**c**) Machine 3.

3.2. Slot-Leakage Component

The coil conductors housed in the stator slot drive the flux not only across the air gap but also across the slot itself. Thus, it results in another inductance component: the slot-leakage component.

(1) Self-inductance

Slot leakage flux in the SSPM machine can be depicted, as shown in Figure 6. As can be seen, the slot leakage due to phase A not only links itself but also links phase B or C for these three machines. In addition, the slot leakage flux passes only one slot either in machine 1 or 3 and three slots in machine 2, which results in a different slot permeance.

The inductance of a single coil is shown as follows:

$$L_{SC} = 2qN_c^2 L_a \Lambda_s \tag{25}$$

where Λ_s is slot permeance, and it can be expressed as follows [29]:

$$\Lambda_s = \mu_0 \left(\frac{2h_s}{3b_{s1} + 3b_{s2}} + \frac{h_0}{b_0} \right) \tag{26}$$

where h_s, b_{s1}, b_{s2}, h_0, and b_0 are illustrated in Figure 6.

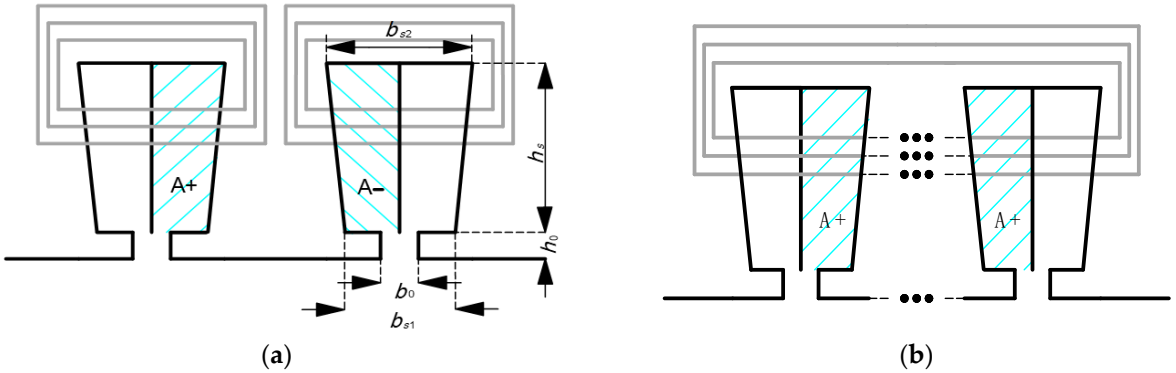


Figure 6. Slot leakage. (**a**) Machine 1 and machine 3. (**b**) Machine 2.

Hence, the permeance for machines 1 and 3 is

$$\Lambda_s = \Lambda_{s1} = \Lambda_{s3} \tag{27}$$

However, since the slot leakage flux passes three slots, the slot permeance of machine 2 is only 1/3 of machine 1 or 3, namely,

$$\Lambda_{s2} = \frac{\mu_0}{3}\left(\frac{2h_s}{3b_{s1}+3b_{s2}} + \frac{h_0}{b_0}\right) \tag{28}$$

Therefore, the slot-leakage component can be obtained as follows:

$$L_{slot} = \frac{N_s}{3} \cdot 2qN_c^2 L_a \Lambda_s = 2qN_c N L_a \Lambda_s \tag{29}$$

(2) Mutual inductance

Mutual inductance due to slot leakage is similar to that due to the air-gap component. As shown in Figure 6, in the three machines, the slot leakage due to one coil side of phase A can link phase B or C. Hence, the mutual inductance can be written as follows:

$$M_{slot} = \frac{N_s}{3} \cdot qN_c^2 L_a \Lambda_s = qN_c N L_a \Lambda_s = \frac{L_{slot}}{2} \tag{30}$$

Therefore, the slot-leakage component for these three machines can be calculated from Equations (29) and (30), and the only difference is slot permeance.

3.3. End-Leakage Component

The end-leakage component, due to the flux leakage of end winding, is usually difficult to evaluate since the end winding is rather complex. The most common way to simplify the end winding configuration is shown in Figure 7, where β is the arc length, which is less than the coil span since the coil sides do not lie exactly on the slot center lines but tend to be closer to the slot wall. The dashed line in the right figure is an imaginary circle flattened by the end windings, and its radius meets $R_e = \beta/2$.

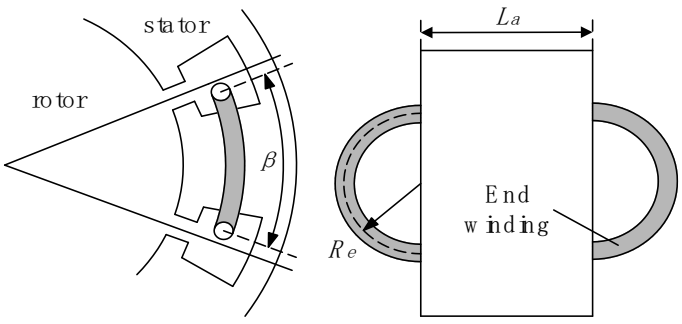


Figure 7. End-leakage calculation.

(1) Self-inductance

End winding leakage can be calculated from Figure 6. According to the literature [24], the end-leakage inductance is calculated by the following:

$$L_{end} = \frac{N_s}{3}\mu_0 R_e N^2{}_c(\ln\frac{8R_e}{R} - 2) = \mu_0 R_e N_c N(\ln\frac{8R_e}{R} - 2) \quad (31)$$

where R_e is the radius of end windings, R is the geometric average distance of the coil side from itself, and it can also be determined by the following equation:

$$R = 0.4394\sqrt{a} \quad (32)$$

where a is the area of the coil side.

(2) Mutual inductance

The model of the mutual inductance of the end-leakage component is the shaded part, as shown in Figure 8, where number 1, 2 and 3 mean coil 1, 2 and 3. Unlike the former mutual inductance components, mutual inductance due to end-winding leakage exists only when the overlapping winding configuration is utilized. Hence, in these three SSPM machines with non-overlapping winding configurations, the mutual inductance due to the end-leakage component is zero.

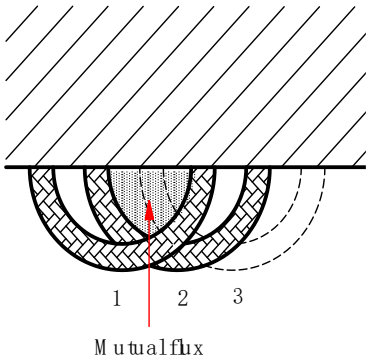


Figure 8. Mutual inductance of end-leakage component.

3.4. FEA Validation

In order to verify the analytical expressions derived above, an FEA evaluation is utilized in this sub-section by setting six SSPM machines as examples. Their key dimensions and parameters are listed in Table 1. It should be noted that both 6/8 and 12/14 machines are FRPM machines with two different magnetization modes. Meanwhile, 6/8 and 12/10 machines are mentioned in Section 2, Figure 3. In addition, according to Equations (16)–(18), the 12/8 and 12/14 machines with magnetization mode 2 have two winding pole pairs, which means these two machines have similar winding configurations to machine 2. Thus, their phase inductances can be calculated according to machine 2, while for the 12/14 machine with magnetization mode 1, its phase inductance can be evaluated according to machine 1 or 3. Therefore, all the inductance data calculated by both FEA and analytical expressions are summarized in Table 2. Clearly, both results agree well.

Table 1. Details of the modeling SSPM machines.

Item	Parameters			
N_s/N_r	6/8	12/8	12/10	12/14
D_{so}/D_{si} (mm)	128/70.4	128/70.4	128/70.4	124/73.5
δ (mm)	0.35	0.35	0.35	0.6
L_a (mm)	75	75	75	120
B_r (T)	1.2	1.2	1.2	1.1
H_c (A/m)	910	910	910	834

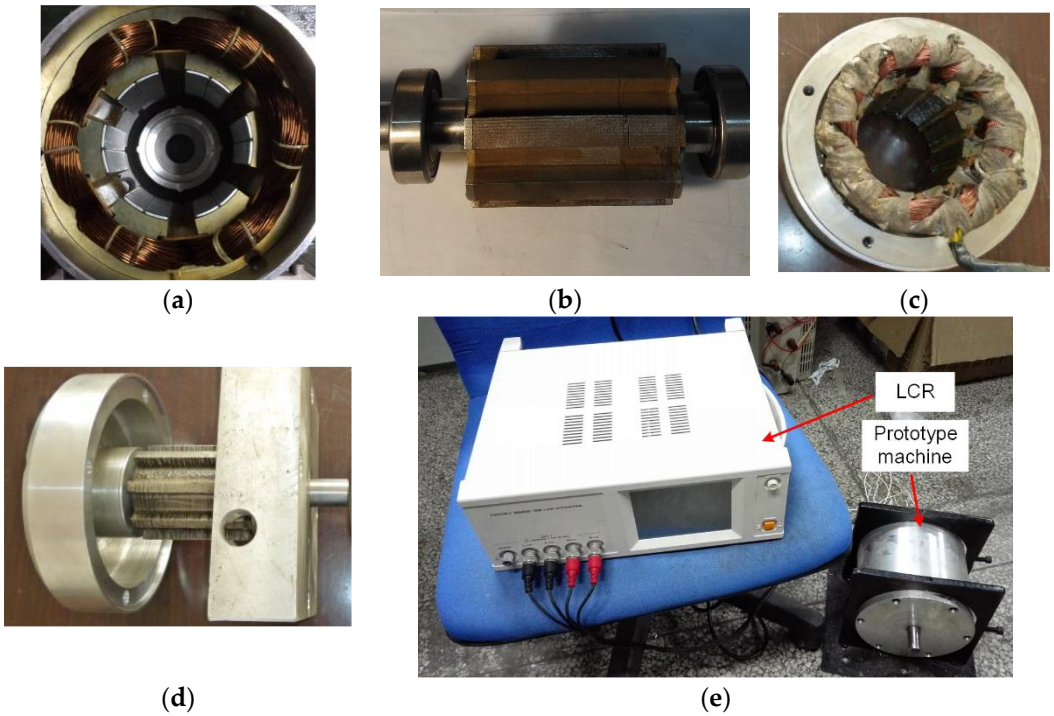
Table 2. Comparison of inductance between analytical and FEA results.

Machine Types		Analytical Component (mH)					Total (mH)		FEA (mH)	
		L_g	M_g	L_{slot}	M_{slot}	L_{end}	L	M	L	M
6/8	mode 1	20.1	0	2.1	1.05	0.9	23.1	1.05	21.2	1.0
	mode 2	10.1	−5.0	3.1	−1.6	0.9	14.1	−6.6	15.7	−6.1
12/8		31.4	0	9.3	−4.7	1.1	41.8	−4.7	40.0	−5.6
12/10		25.5	−12.8	22.6	−11.3	3.0	51.1	−24.1	56.4	−24.7
12/14	mode 1	6.4	−3.2	8.0	−4.0	1.0	15.4	−7.2	16.8	−7.0
	mode 2	12.7	0	5.3	2.7	1.0	19.0	2.7	21.2	2.6

4. Experimental Validation

4.1. Prototype Machines and Platform Setup

In this section, in order to verify the analytical results of the above-mentioned inductances, three SSPM machines, including two 6/8 machines with different magnetization modes (Figure 1c,d) and a 12/10 machine, are manufactured, as shown in Figure 9. It should be noted that the two 6/8 machines are completely the same except for the magnetization mode and winding configuration, as shown in Figure 1. In addition, Figure 9e shows the experimental setup that contains an inductance detector and a prototype. The inductance detector is utilized to measure the inductance data, and it is made by the HIOKI 3522-50 LCR Hitester, which is short for LCR in this paper.



(**a**) (**b**) (**c**) (**d**) (**e**)

Figure 9. Prototype machines. (**a**) Stator (6/8). (**b**) Rotor (6/8). (**c**) Stator (12/10). (**d**) Rotor (12/10). (**e**) Experimental platform.

4.2. Self-Inductance

Self-inductance can be obtained by the testing technique shown in Figure 10, where A denotes the winding of phase A and o, o′ corresponds to the terminals of phase A, which are connected with LCR during the test.

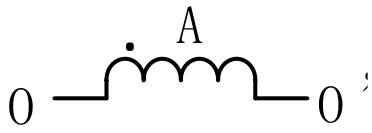


Figure 10. Self-inductance testing system.

4.3. Mutual Inductance

Unlike self-inductance, mutual inductance cannot be acquired directly by the LCR. The testing scheme of mutual inductance is presented in Figure 11, where phases A and B are connected in series. It should be noted that the dotted terminals must not be connected directly. Thus, the total inductance of phases A and B can be acquired, through which the mutual inductance can be calculated by the following equation:

$$M_{ab} = \frac{L_{\text{total}} - L_a - L_b}{2} \tag{33}$$

where L_{total} is the total inductance acquired from the scheme shown in Figure 11; L_a and L_b are the self-inductances of phase A and phase B, respectively, which can be obtained in Figure 10.



Figure 11. Mutual inductance testing system.

4.4. Inductance Data

Through the techniques mentioned above, both self- and mutual inductances can be obtained by setting phase A as an example (Figure 12). Meanwhile, the FEA-predicted and analytical results are also presented for contrast. It should be noted that the analytical results are straight lines since only the position shown in Figure 3 was analyzed. As can be seen, the analytical results agree with both FEA-predicted and tested data very well. More details are listed in Table 3. In addition, it can also be found that the error of FEA-predicted results is smaller since it considers both flux leakage and magnetic saturation.

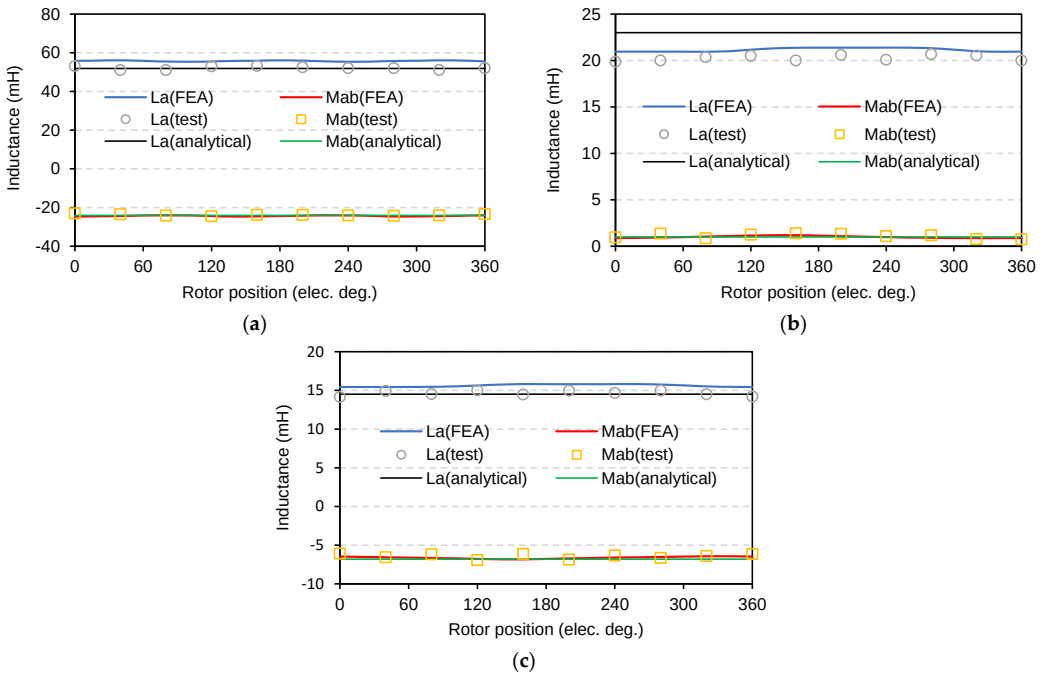


Figure 12. Self- and mutual inductances of three prototyped SSPM machines. (**a**) Machine 1. (**b**) Machine 2. (**c**) Machine 3.

Table 3. Comparison of the inductance Results from different techniques.

Machine Types		Analytical (mH)		FEA (mH)		Measured (mH)		Error Analytical		Error FEA	
		L	*M*	*L*	*M*	*L*	*M*	*L*	*M*	*L*	*M*
6/8	mode 1	23.1	1.05	21.2	1.0	21.5	1.01	7.4%	4%	1.4%	1%
	mode 2	14.1	−6.6	15.7	−6.1	15.1	−6.3	6.6%	4.8%	4%	3.2%
12/10		51.1	−24.1	56.4	−24.7	54.1	−24.9	5.5%	3.2%	4.3%	0.8%

5. Conclusions

Based on a magneto motive force (MMF)-permeance model, the winding configurations and winding pole pairs for SSPM machines can be determined. According to the winding configuration, phase inductance can be analytically derived, which agrees well with the FEA and experiment. In addition, it is found that the winding inductances in the SSPM machine are almost rotor-position-independent, which means that the 'id = 0' control strategy can be used.

Author Contributions: Writing—review & editing, X.Z. and Y.Y. All authors have read and agreed to the published version of the manuscript.

Funding: This research was funded by National Natural Science Foundation of China grant number 52107050.

Data Availability Statement: The original contributions presented in the study are included in the article, further inquiries can be directed to the corresponding author.

Conflicts of Interest: The authors declare no conflict of interest.

References

1. Shao, L.; Hua, W.; Dai, N.; Tong, M.; Cheng, M. Mathematical modeling of a 12-phase flux-switching permanent-magnet machine for wind power generation. *IEEE Trans. Ind. Electron.* **2015**, *63*, 504–516. [CrossRef]
2. Wang, Y.; Deng, Z. Comparison of switched-flux permanent magnet machines with non-overlapping concentrated winding for open-winding generator system. *IET Electr. Power Appl.* **2017**, *11*, 242–251. [CrossRef]
3. Gao, Y.; Qu, R.; Li, D.; Chen, F. Force ripple minimization of a linear vernier permanent magnet machine for direct-drive servo applications. *IEEE Trans. Magn.* **2017**, *53*, 7001905. [CrossRef]
4. Yang, T.; Chau, K.; Liu, W.; Ching, T.; Cao, L. Comparative analysis and design of double-rotor stator-permanent-magnet motors with magnetic-differential application for electric vehicles. *World Electr. Veh. J.* **2022**, *13*, 199. [CrossRef]
5. Hua, W.; Zhang, H.; Cheng, M.; Meng, J.; Hou, C. An outer-rotor flux-switching permanent-magnet-machine with wedge-shaped magnets for in-wheel light traction. *IEEE Trans. Ind. Electron.* **2017**, *64*, 69–80. [CrossRef]
6. Fei, W.; Luk, P.C.K.; Shen, J.X.; Wang, Y.; Jin, M. A novel permanent-magnet flux switching machine with an outer-rotor configuration for in-wheel light traction applications. *IEEE Trans. Ind. Appl.* **2012**, *48*, 1496–1506. [CrossRef]
7. Jing, L.; Yang, K.; Gao, Y.; Kui, Z.; Min, Z. Analysis and optimization of a novel flux reversal machine with auxiliary teeth. *Energies* **2022**, *15*, 8906. [CrossRef]
8. Ding, Z.; He, C.; Feng, C.; Yang, J. A new dual stator permanent magnet machine based on field modulation theory. *Sustainability* **2022**, *15*, 281. [CrossRef]
9. Hua, W.; Su, P.; Shi, M.; Zhao, G.; Cheng, M. The influence of magnetizations on bipolar stator surface-mounted permanent magnet machines. *IEEE Tran. Magn.* **2015**, *51*, 8201904.
10. Zhang, Y.; Hua, W.; Cheng, M.; Zhang, G.; Fu, X. Static characteristic of a novel stator surface-mounted permanent magnet machine for brushless DC drives. In Proceedings of the IECON 2012–38th Annual Conference of IEEE Industrial Electronics, Montreal, QC, Canada, 25–28 October 2012; pp. 4139–4144.
11. Manne, B.; Kumar, M.; Akuru, U. Design and Performance Assessment of a Small-Scale Ferrite-PM Flux Reversal Wind Generator. *Energies* **2020**, *13*, 5565. [CrossRef]
12. Zhu, X.; Hua, W. Back-EMF waveform optimization of flux-reversal permanent magnet machines. *AIP Adv.* **2017**, *7*, 056613. [CrossRef]
13. Gao, Y.; Qu, R.; Li, D.; Li, J.; Zhou, G. Consequent-pole flux-reversal permanent-magnet machine for electric vehicle propulsion. *IEEE Trans. Appl. Supercond.* **2016**, *26*, 5200105. [CrossRef]
14. Huang, W.; Hua, W.; Yu, F. Improved model-predictive-flux-control strategy for three-phase four-switch inverter-fed flux-reversal permanent magnet machine drives. *IET Elect. Power Appl.* **2017**, *11*, 717–728.

15. Gao, Y.; Qu, R.; Li, D.; Li, J. Torque performance analysis of three-phase flux reversal machines. *IEEE Tran. Ind. Appl.* **2017**, *53*, 2110–2119. [CrossRef]
16. Dmitrievskii, V.; Prakht, V.; Kazakbaev, V. Novel rotor design for high-speed flux reversal motor. *Energy Rep.* **2020**, *6*, 1544–1549. [CrossRef]
17. Zhao, G.; Hua, W.; Zhu, X.; Zhang, G. The influence of dummy slots on stator surface-mounted permanent magnet machines. *IEEE Tran. Magn.* **2017**, *53*, 7207105. [CrossRef]
18. Yu, Y.; Nakamura, K. Prototype Verification of Flux Reversal Motor with Cross-Pole Shape Stator. *IEEE Trans. Magn.* **2024**, *60*, 8204205. [CrossRef]
19. Zheng, Y.; Xiang, W.; Xu, H.; Tan, P.; Fang, Y. Analysis of a Flux Reversal Machine with Consequent-Pole Evenly Distributed PM. *IEEE Tran. Ind. Appl.* **2023**, *60*, 4–11. [CrossRef]
20. Bi, Y.; Fu, W.; Niu, S.; Huang, J. Comparative analysis of consequent-pole flux-switching machines with different permanent magnet arrangements for outer-rotor in-wheel direct-drive applications. *Energies* **2023**, *16*, 6650. [CrossRef]
21. Gao, Y.; Qu, R.; Li, D.; Li, J. Design procedure of flux reversal permanent magnet machines. *IEEE Tran. Ind. Appl.* **2017**, *53*, 4232–4241. [CrossRef]
22. Hua, H.; Zhu, Z.Q. Flux Reversal Permanent Magnet Machines with Single-Layer Non-Overlapping Windings. *IEEE Tran. Energy Convers.* **2023**, *38*, 1521–1529. [CrossRef]
23. El-Refaie, A.M.; Zhu, Z.Q.; Jahns, T.M.; Howe, D. Winding inductances of fractional slot surface-mounted permanent magnet brushless machines. In Proceedings of the 2008 IEEE Industry Applications Society Annual Meeting, Alberta, AB, Canada, 5–9 October 2008; pp. 1–8.
24. Hendershot, J.R.; Miller, T.J.E. *Design of Brushless Permanent-Magnet Machines*; Magna Physics Publishing: Lebanon, OH, USA; Oxford University Press: Oxford, UK, 1994.
25. Cai, S.; Chen, H.; Yuan, X.; Wang, Y.; Shen, J.; Lee, C. Analysis of Synergistic Stator Permanent Magnet Machine with the Synergies of Flux-Switching and Flux-Reversal Effects. *IEEE Tran. Ind. Electron.* **2022**, *69*, 12237–12248. [CrossRef]
26. El-Refaie, A.M.; Jahns, T.M.; McCleer, P.J.; McKeever, J.W. Experimental verification of optimal flux weakening in surface PM machines using concentrated windings. *IEEE Tran. Ind. Appl.* **2006**, *42*, 443–453. [CrossRef]
27. Conradi, A.; Schmidt, D.; Deeg, C. Contribution to the analysis of end winding inductances of induction machines. In Proceedings of the 2016 XXII International Conference on Electrical Machines (ICEM), Lausanne, Switzerland, 4–7 September 2016; pp. 245–251.
28. Dutta, R.; Rahman, M.F.; Chong, L. Winding inductances of an interior permanent magnet (IPM) machine with fractional slot concentrated winding. *IEEE Trans. Magns.* **2012**, *48*, 4842–4849. [CrossRef]
29. Chen, S. *Design of Electrical Machines*; China Machine Press: Beijing, China, 2000.

Disclaimer/Publisher's Note: The statements, opinions and data contained in all publications are solely those of the individual author(s) and contributor(s) and not of MDPI and/or the editor(s). MDPI and/or the editor(s) disclaim responsibility for any injury to people or property resulting from any ideas, methods, instructions or products referred to in the content.